https://doi.org/10.5194/essd-2025-438
Preprint. Discussion started: 13 August 2025

Open Access Earth System Science Data Discussions

High-Quality Remote Sensing Reflectance Products over China and US Coast

Shuhui Zhao[1,2], Youlv Wu[3,4], Jingning Lv[1], Dan Zhao[1], Yan Zheng[1], Lian Feng[2]

[1]School of Environmental Science and Engineering, Southern University of Science and Technology, Shenzhen, 518055, China
[2]State Key Laboratory of Information Engineering in Surveying, Mapping and Remote Sensing, Wuhan University, Wuhan, China
[3]School of Environmental Science and Engineering, Shanghai Jiao Tong University, Shanghai, 200240, China
[4]School of the Environment and Sustainable Engineering, Eastern Institute of Technology, Ningbo, 315200, China

Correspondence to: Lian Feng (lianfeng619@gmail.com)

Abstract Remote sensing reflectance (R_{rs}) is fundamental for deriving bio-optical properties of global surface waters. However, accurate atmospheric correction (AC) to derive R_{rs} in coastal waters remains challenging due to strongly absorbing aerosols and complex water optics. To address this, we developed an improved processing framework that integrates flexible use of global gridded aerosol models better suited for coastal environments and incorporates tailored masking strategies. Based on this framework, we generated a high-quality R_{rs} dataset from Moderate Resolution Imaging Spectroradiometer (MODIS) Aqua observations, spanning 2003–2022 for the coastal waters of China and the United States (US)—two regions where complex water optics and frequent anthropogenic aerosols have long impeded retrieval accuracy and valid data yield. Compared to the NASA standard MODIS Aqua R_{rs} products (mean regression slope: 0.90 ± 0.06), the improved framework achieves higher accuracy and reduced overcorrection biases (slope: 1.00 ± 0.08) across eight bands, especially in the 488–555 nm range. The new dataset also yields significantly more valid retrievals, with regional mean increases of 56% in the Chinese coastal waters and 18% in the US coastal waters at 443 nm. Regional image analyses confirm its superior capability in preserving valid retrievals and resolving fine-scale spatial features in turbid nearshore waters. Preliminary spatiotemporal analyses further demonstrate its effectiveness in capturing long-term R_{rs} dynamics and trends. These results highlight the robustness of the improved framework and the practical utility of the new dataset for long-term monitoring of coastal water quality and ecosystem variability. The dataset is available at https://doi.org/10.5281/zenodo.16413443 (Zhao et al., 2025).

1 Introduction

Remote sensing reflectance (R_{rs}), representing the fraction of the top-of-atmosphere (TOA) signal attributable to water-leaving radiance (Gordon, 1997), is fundamental for deriving bio-optical properties of global surface waters, such as inherent optical properties (IOPs) (Lee et al., 2002; Werdell et al., 2013), concentrations of chlorophyll-a (Chl) (O'reilly, 2000; Hu et al., 2019; Tong et al., 2022) and particulate organic carbon (POC) (Stramski et al., 1999; Stramski et al., 2022), among many others. Accurate atmospheric correction (AC)—which removes atmospheric contributions from the total radiance measured by

https://doi.org/10.5194/essd-2025-438
Preprint. Discussion started: 13 August 2025

satellite sensors—is critical for retrieving R_{rs} and estimating water quality parameters (Gordon and Wang, 1994; Gordon, 1997). However, a key challenge in AC lies in accurately characterizing aerosol radiative properties, especially in the presence of absorbing aerosols which strongly absorb light at short blue bands (410 or 412 nm and 443 nm) (Bassani et al., 2015; Ioccg, 2019). In coastal regions where such aerosols (e.g., dust, smoke, and urban aerosols) are prevalent (Charlson et al., 1992), the aerosol models developed by Ahmad et al. (2010) (hereafter referred to as AF10), which are widely used in current operational AC, fail to account for strong aerosol absorption (Zhao et al., 2023), leading to systematic underestimation and limited reliability of R_{rs} (Wang and Jiang, 2018). In addition to aerosol-related issues, the cloud mask applied in current ocean color data processing pipelines often misclassifies highly reflective turbid waters (e.g., those with high suspended sediment concentrations) as clouds, resulting in the loss of usable R_{rs} data in coastal regions (Wang and Shi, 2006). Together, these issues severely constrain the usability of R_{rs} products in coastal regions and hamper the accurate retrieval of biogeochemical properties in these dynamic environments.

One of the key factors determining the accuracy of R_{rs} retrievals after atmospheric correction is whether the adopted aerosol models can effectively capture the microphysical and optical properties of aerosols, thereby accurately estimating their scattering contributions (Prospero et al., 1983; Gordon et al., 1997; Bassani et al., 2015). To address this, a range of aerosol models has been developed and refined by incorporating observational data and analyzing aerosol sources (Shettle and Fenn, 1979; Gordon and Wang, 1994; Ahmad et al., 2010; Zhao et al., 2023). Early work by Shettle and Fenn (1979) classified aerosols into five types (rural, urban, maritime, tropospheric, and fog) and accounted for humidity effects to produce a set of models (denoted as SF79). Building on this, Gordon and Wang (1994) formulated 12 humidity-dependent aerosol models (denoted as GW94) tailored for marine applications. With improved observational capacity, Ahmad et al. (2010) developed the AF10 models based on long-term data from 11 AErosol RObotic NETwork (AERONET) sites. The AF10 models parameterize aerosol particle size, refractive index, and fine-mode fraction as functions of relative humidity. Compared to GW94, they significantly reduced the uncertainties in aerosol optical thickness (AOT) and Ångström exponent (He et al., 2011; Mélin et al., 2013). As a result, the AF10 models have become the default aerosol model set in most current operational ocean color data processing systems (Mobley et al., 2016).

However, current operational AC based on AF10 models frequently yield poor R_{rs} retrievals in coastal regions, often resulting in underestimated R_{rs} values, particularly in the blue bands (Wang and Jiang, 2018). This limitation stems from the spatial representativeness of the AERONET sites used to build AF10 models: only three coastal stations (all in Chesapeake Bay) were included, while the remaining sites were located over open oceans. As a result, AF10 models primarily represent non- or weakly absorbing aerosols over the open ocean, and do not adequately reflect the high AOT and strong absorption features commonly present in coastal regions (Zhao et al., 2023). Although many studies have proposed aerosol model refinements (Giles et al., 2012; Hamill et al., 2016; Bru et al., 2017; Zhou et al., 2020; Montes et al., 2022), most focus on specific aerosol types or lack representation of seasonal variability, limiting their broader applicability for coastal waters.

https://doi.org/10.5194/essd-2025-438
Preprint. Discussion started: 13 August 2025

Recognizing the limitations of the AF10 models, Zhao et al. (2023) developed a set of global gridded aerosol models tailored for inland and coastal waters. Leveraging AERONET observations from 1,475 sites worldwide, they generated 3,207 monthly aerosol models distributed across 310 5°×5° grids, and compiled the models into lookup tables compatible with the Sea-viewing Wide Field-of-view Sensor (SeaWiFS) Data Analysis System (SeaDAS) to allow seamless integration into operational AC workflows. Validation using Moderate Resolution Imaging Spectroradiometer (MODIS) Aqua data over six lacustrine or estuarine regions showed that the gridded models substantially improved R_{rs} retrieval accuracy compared to the AF10 models. Recently, Lv et al. (2024) further demonstrated the robustness of the gridded models through extended validations across multiple coastal regions and MODIS bands, with notable reductions in aerosol overcorrection errors under complex aerosol conditions.

Although such global gridded aerosol models have shown promise in characterizing the complex aerosol properties of coastal regions, several practical challenges hinder their direct application in operational coastal R_{rs} product generation. One key limitation lies in the intrinsic complexity of coastal environments, where both atmospheric and water optical conditions can exhibit strong spatial heterogeneity within a single satellite scene—from nearshore turbid waters dominated by strongly absorbing continental aerosols to offshore regions with clearer water and weakly absorbing marine aerosols. Applying either model type uniformly across such spatial gradients can lead to potential retrieval errors—for instance, using AF10 models nearshore often results in overestimated aerosol path radiance and underestimated R_{rs}, while applying the gridded models offshore may produce unrealistically high R_{rs} values due to overestimated aerosol absorption. These challenges highlight the necessity of developing a dynamic and integrated model selection scheme that can adaptively select between gridded and AF10 aerosol models under spatially heterogeneous conditions, to support accurate AC across the full coastal domain and generate spatially consistent, quality-assured R_{rs} products suitable for large-scale analysis.

In addition to aerosol model selection issues, a more suitable cloud masking strategy is also essential for improving the usability of coastal R_{rs} data. The default cloud mask employed in current operational processing workflows—originally designed for open-ocean applications—relies on a Rayleigh reflectance threshold at 869 nm ($R_{rc,869}$ = 0.027) to identify cloudy pixels (Robinson et al., 2003). However, in turbid coastal waters, this threshold can easily be exceeded due to high water-leaving radiance, leading to misclassification of valid pixels as cloudy (Wang and Shi, 2006). As a result, a substantial portion of valid data was incorrectly discarded, limiting the spatial coverage and continuity of the standard R_{rs} products. To address this, previous studies have proposed using alternative thresholds at 1240 or 2130 nm, as these relaxed cloud masking thresholds help retain more turbid water pixels. However, the relaxation of the cloud masking criteria may increase the risk of residual contamination from thin clouds. Therefore, targeted masking approaches must be incorporated during data processing to complement the modified cloud masking threshold, thereby ensuring data reliability.

In summary, while prior studies have addressed two major limitations of standard R_{rs} products in coastal waters—namely, the inadequacy of aerosol models and the excessive cloud masking—these improvements have yet to be fully integrated into

https://doi.org/10.5194/essd-2025-438
Preprint. Discussion started: 13 August 2025

operational data production. To bridge this gap, we developed an improved processing framework that integrates refined aerosol model assignment and targeted masking strategies. To evaluate its performance, we conducted MODIS satellite–*in situ* matchup validation on a global scale and compared with the standard R_{rs} products. We further applied the improved framework to generate a consistent and high-quality MODIS R_{rs} dataset for two representative coastal regions—the coastal waters of China and the United States (US)—both of which are characterized by optically complex waters, strong anthropogenic influences, and insufficient data availability (Charlson et al., 1992; Wang et al., 2017). Evaluation of data coverage and spatiotemporal analyses were conducted using the new dataset to assess its utility to provide a consistent and high-quality basis for long-term coastal monitoring and regional change detection.

2 Data and Methods

2.1 Datasets

2.1.1 Satellite Imagery

This study utilized two types of MODIS Aqua satellite data acquired from the NASA Ocean Biology Processing Group (https://oceancolor.gsfc.nasa.gov/): Level-1A (L1A) and Level-2 (L2) ocean color products. L1A products contain unprocessed full-resolution data, supplemented with radiometric and geometric calibration coefficients and georeferencing parameters. L2 products provide derived geophysical variables (e.g., R_{rs}, Chl) at the same spatial resolution and geolocation as L1A data.

A total of 136,544 L1A images acquired between 2002 and 2022 (data beyond 2022 were excluded here due to satellite orbital changes beginning in 2023 (Twedt et al., 2023; Nasa Ocean Biology Processing Group, 2024)) were used in this study for two main purposes:

(1) Matchup validation: A subset of 4,961 L1A images (2002-2022) was used to generate satellite R_{rs} for validation against *in situ* measurements, with temporal coverage aligned to field campaigns.
(2) New coastal R_{rs} dataset generation: Most of the images (128,226 scenes, from 2003 to 2022) were used to generate the new R_{rs} dataset for two regions: the coastal waters of Chinese mainland (106°E–127°E, 17°N–41°N) and the US (128°W–65°W, 18°N–51°N).

NASA standard Level-2 R_{rs} products generated using the operational AC algorithm developed by NASA OBPG (Nasa Ocean Biology Processing Group, 2022) were also obtained. This dataset was used for:

(1) Comparative validation with R_{rs} data generated in this study using a common set of *in situ* measurements.
(2) Evaluation of improvements in valid data yield by comparing valid observations counts (see Sect. 2.3.2) and assessing single-scene retrievals.

https://doi.org/10.5194/essd-2025-438
Preprint. Discussion started: 13 August 2025

Both the new dataset and standard products include R_{rs} at 10 spectral bands: 412, 443, 469, 488, 531, 547, 555, 645, 667, and 678 nm, all at 1 km spatial resolution.

2.1.2 Ancillary Environmental Data

To support accurate AC, this study also incorporated ancillary data (Nasa Ocean Biology Processing Group, 2019) during the processing of MODIS imagery. These inputs—automatically acquired via the SeaDAS processing environment—include meteorological variables (e.g., wind speed, surface pressure, relative humidity) and concentrations of atmospheric gases (e.g., water vapor, ozone, nitrogen dioxide). These parameters are essential for calculating Rayleigh scattering, atmospheric transmittance, and gaseous absorption, and thus directly influence the quality of retrieved R_{rs} values. The best available ancillary data at the time of processing were used, consistent with standard SeaDAS ancillary data usage practices. This approach helps minimize the influence of auxiliary input differences when comparing with the standard R_{rs} products and improves the reliability of R_{rs} values derived with our improved processing framework.

2.1.3 *In Situ* Data

To evaluate the performance of the improved processing framework and compare its outputs with the standard products, we used *in situ* R_{rs} measurements archived in the SeaWiFS Bio-optical Archive and Storage System (SeaBASS, http://seabass.gsfc.nasa.gov/) (Werdell et al., 2003; Bailey and Werdell, 2006). SeaBASS provides precompiled satellite–*in situ* matchup records, each containing metadata such as geographic coordinates, sampling time, cruise ID, measured R_{rs} values, corresponding MODIS Aqua filenames, and validation flags. In this study, the metadata was used to extract satellite-derived R_{rs} from outputs of our improved processing framework and standard products, rather than using the satellite R_{rs} values directly included in the SeaBASS records. This allowed us to apply a unified and more stringent quality control (QC) strategy (see Sect. 2.2.2) to both data, ensuring consistency and reliability of the accuracy assessment.

The *in situ* measurements cover eight MODIS bands: 412, 443, 488, 531, 547, 555, 667, and 678 nm. Due to a lack of *in situ* records at 469 and 645 nm, these two bands were excluded from all accuracy assessments (see Sect. 2.3.1).

To focus on coastal conditions and ensure compatibility with the coverage of the global gridded aerosol models, observations located over open ocean or inland waters were excluded. A total of 6,362 *in situ* records were retained for validation, distributed across a wide range of coastal environments (see Figure 1).

https://doi.org/10.5194/essd-2025-438
Preprint. Discussion started: 13 August 2025

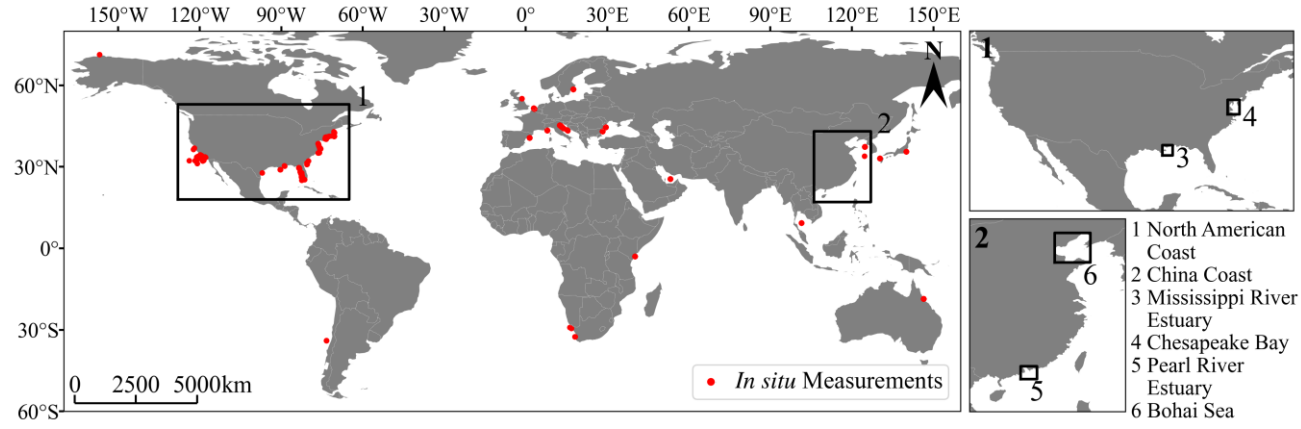

Figure 1: Distribution of *in situ* measurements. Also shown are the study areas—the coastal waters of China and the United States—as well as four specific regions of interest: the Mississippi River Estuary, Chesapeake Bay, Pearl River Estuary, and Bohai Sea.

2.2 Processing Framework

Accurate AC is essential for deriving reliable R_{rs} in optically complex coastal waters, where high turbidity and variable aerosol properties present persistent challenges. In this study, we refined current operational ocean color AC algorithm (Mobley et al., 2016) to enhance its performance in such environments. All processing was conducted using SeaDAS software (version 8.3.0).

Our modifications build upon the standard near-infrared (NIR) iterative approach, which estimates aerosol contributions by assuming negligible water-leaving radiance in the NIR bands and minimizing residual signals through iteration (Gordon and Wang, 1994; Mobley et al., 2016). While effective over open ocean, this method could produce biased results in coastal waters due to sharp gradients in both water optical properties and aerosol characteristics. To address these limitations, we introduced a more flexible AC approach tailored to spatially heterogeneous coastal conditions. The full procedure is detailed in Sect. 2.2.1.

Additionally, a unified set of QC strategies was applied to both the newly generated data in this study and standard R_{rs} products to ensure consistency in evaluation. These procedures are described in Sect. 2.2.2.

2.2.1 Improved Atmospheric Correction

Building upon the standard NIR iterative approach, we further enhanced AC performance in coastal waters by incorporating the global gridded aerosol models (Zhao et al., 2023) and introducing a spatially adaptive aerosol model selection strategy. The overall process is illustrated in Figure 2.

https://doi.org/10.5194/essd-2025-438
Preprint. Discussion started: 13 August 2025

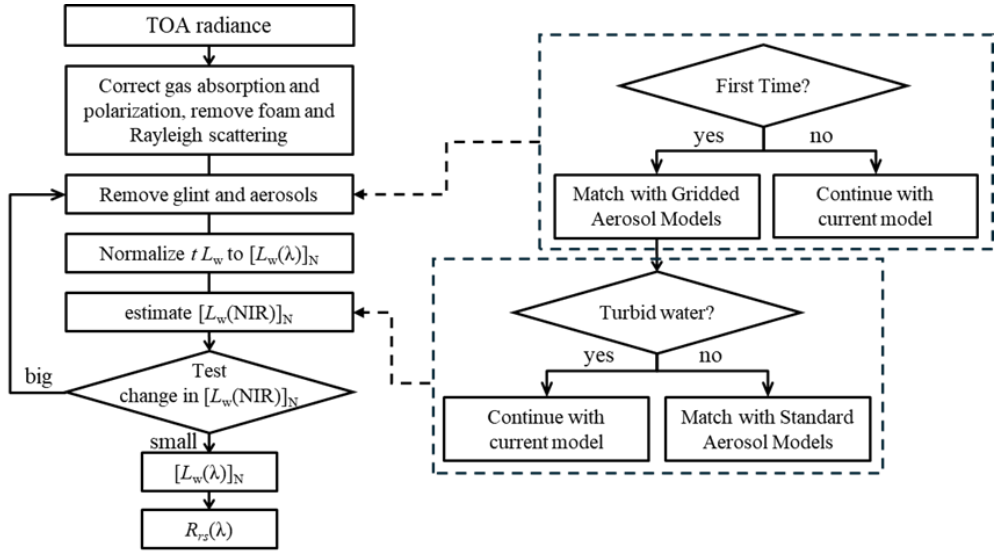

Figure 2: Improved atmospheric correction (AC) workflow. Notation: t (diffuse transmittance), L_w (water-leaving radiance), λ (wavelengths), NIR (near-infrared), N (normalization).

After preprocessing steps such as Rayleigh scattering and sun glint removal, the initial aerosol contribution was estimated using a gridded aerosol model selected based on the pixel's geographic location and date (Zhao et al., 2023), since the gridded models offer improved representation of the diverse and potentially absorbing aerosols common in coastal regions.

To account for spatial heterogeneity in coastal conditions, each pixel was preliminarily classified based on its normalized NIR water-leaving radiance (denoted as $[L_w(NIR)]_N$). Specifically, a pixel was classified as "turbid" if $[L_w(NIR)]_N$ exceeded the empirical threshold defined by the TURBIDW flag in NASA Standard Level-2 Ocean Color Flags. Although this classification nominally distinguishes between clear and turbid waters, it served here primarily as a proxy for proximity to land. Turbid waters—characterized by elevated NIR reflectance due to high concentrations of suspended sediments or phytoplankton—are typically concentrated in nearshore zones, where riverine input and absorbing aerosols from anthropogenic sources are most pronounced (Husar et al., 1997). For these pixels, the gridded aerosol model originally assigned to the location was retained throughout iteration to better represent local aerosol properties. In contrast, pixels classified as "clear" were generally located offshore, where continental aerosol influence is weaker and water clarity is higher. For these pixels, an AF10 aerosol model was selected following the conventional open-ocean AC algorithm and used in subsequent iterations, as continued use of the gridded model in such areas could lead to underestimation of aerosol path radiance and overestimation of water-leaving radiance. This spatially adaptive model selection approach—guided by an indirect indicator of coastal influence—was key to improving retrieval performance across diverse coastal environments.

https://doi.org/10.5194/essd-2025-438
Preprint. Discussion started: 13 August 2025

The iteration proceeded until the change in $[L_w(NIR)]_N$ between successive steps fell below a set threshold, after which the final $[L_w(\lambda)]_N$ was converted to $R_{rs}(\lambda)$.

While the NIR-SWIR switching method is considered more robust for highly turbid waters—leveraging the near-zero water-leaving radiance assumption in the shortwave infrared (SWIR) bands—it is constrained by the low signal-to-noise ratios (SNR) of MODIS Aqua SWIR bands (Wang et al., 2009; Werdell et al., 2010). As demonstrated in previous studies (Shi and Wang, 2007; Wang et al., 2009) and confirmed by our tests, excessive noise in these bands can significantly compromise retrieval accuracy. Therefore, we retained the NIR iterative approach, with enhanced reliability achieved through spatially adaptive aerosol model selection.

2.2.2 Quality Control Strategies

To ensure reliability and comparability of R_{rs} retrievals, a unified set of QC strategies was applied to both the newly generated data in this study and standard products prior to subsequent analysis. These procedures aimed to eliminate contaminated or highly uncertain retrievals and to support robust evaluation of data accuracy and comparison of valid data yield.

NASA Standard Level-2 Ocean Color Flags (l2_flags) were used to mask pixels affected by clouds, ice, sun glint, stray light, and extreme solar or sensor viewing angles. In addition, pixels flagged as MAXAERITER, indicating that the maximum number of aerosol iterations was reached without convergence, were also excluded to minimize the influence of potential AC failure under complex water or aerosol conditions.

Among these flags, the CLDICE mask was customized to improve cloud detection performance over turbid coastal waters. A revised threshold of $R_{rc,2130} = 0.037$ was applied to reduce excessive cloud masking over areas with high AOT and turbid waters (Zhao et al., 2023; Zhang et al., 2014). In contrast, the standard R_{rs} products used for comparison was originally generated with the conventional $R_{rc,869} = 0.027$ threshold.

To further suppress residual cloud contamination that may result in abnormally elevated R_{rs} values, a secondary spectral filter was applied. Specifically, any TURBIDW-flagged pixel with R_{rs} in any of the four blue bands (412–488 nm) exceeding the value at 531 nm was excluded. This criterion effectively identifies cloud-contaminated water pixels whose spectral shapes deviate from typical turbid water profiles—characterized by a reflectance peak near the green wavelengths and decreasing reflectance toward the blue, due to strong absorption by colored dissolved organic matter (CDOM) and Chl (Kirk, 2010). In contrast, cloud-contaminated pixels often exhibit spuriously enhanced blue-band reflectance, resulting in anomalous spectral peaks uncharacteristic of true turbid waters. This filter is hereafter referred to as the “Wrong Turbid Water Mask”.

Extremely turbid waters were also excluded to reduce uncertainty in AC performance. Specifically, pixels exhibiting saturated R_{rs} signals in the 667 nm band—typically associated with very high suspended sediment concentrations—were filtered out, as such conditions compromise the reliability of both aerosol estimation and water-leaving radiance retrievals (Hu et al., 2012). This step is referred to as the “Saturated R_{rs}(667) Mask”.

https://doi.org/10.5194/essd-2025-438
Preprint. Discussion started: 13 August 2025

By applying these QC strategies consistently across both datasets, we ensured that subsequent analyses were based on equivalently screened, quality-assured R_{rs} products.

2.3 Data Usability Assessment

2.3.1 Accuracy Evaluation

To assess the accuracy of the R_{rs} data derived with our processing framework and compare it with standard products, satellite–*in situ* matchups were compiled following NASA OBPG protocols (Bailey and Werdell, 2006). As mentioned in Sect. 2.1.3, both two kinds of satellite R_{rs} values were re-extracted based on the SeaBASS-provided metadata (e.g., geographic coordinates, acquisition time), with the same stricter QC strategy (Sect. 2.2.2) applied to ensure comparability.

Matchups were identified based on a ±3-hour temporal window between satellite overpass and *in situ* measurement. To ensure spatial representativeness and minimize the impact of pixel-level variability, a 5×5 pixel window centered on the *in situ* location was extracted from each satellite image. Within each window, only non-land pixels were considered. A matchup was deemed valid only if more than 50% of the pixels in the window passed QC screening and the coefficient of variation (standard deviation divided by the mean) was below 0.15—ensuring spatial homogeneity and consistency with *in situ* conditions.

R_{rs} accuracy was evaluated using four metrics: regression slope, coefficient of determination (R^2), median absolute percentage error (MdAPE), and normalized root mean square error (NRMSE). Among them, MdAPE serves as a robust indicator of relative error, being less sensitive to outliers than MAPE (mean absolute percentage error). NRMSE provides a scale-independent measure suitable for cross-band error comparison. These metrics were calculated as follows:

$$MdAPE = median(\left|\frac{Y_i - X_i}{X_i}\right| \times 100\%)$$

$$NRMSE = \frac{\sqrt{\frac{1}{N}\sum_{i=1}^{N}(Y_i - X_i)^2}}{(X_{max} - X_{min})} \times 100\%$$

where X_i and Y_i denote the *in situ* and satellite-derived R_{rs} values respectively, and N is the number of valid matchups.

2.3.2 Valid Data Yield Comparison

Because valid R_{rs} retrievals are often restricted by atmospheric conditions and QC thresholds (Wang and Shi, 2006; Ioccg, 2010), the frequency with which a dataset provides usable values serves as a practical indicator of its spatiotemporal utility. To quantify differences in data availability between the new dataset for coastal waters of China and US and the standard products, we computed a pixel-level metric representing the number of days with valid R_{rs} retrievals throughout the analysis period. For each pixel and spectral band, the number of days with valid retrievals was counted and denoted as VO (Valid Observation). A retrieval was considered valid if the R_{rs} value was non-negative and passed all QC filters described in Sect. 2.2.2.

https://doi.org/10.5194/essd-2025-438
Preprint. Discussion started: 13 August 2025

The difference in valid observation counts between the two datasets was defined as:

$$VOD = VO_{New} - VO_{Standard}$$

Here, VOD (Valid Observation Difference) captures the pixel-wise and band-wise difference in the number of valid retrieval days between the new and standard datasets. A positive VOD indicates that the new dataset provided valid R_{rs} values on more days than the standard dataset at the specific pixel and spectral band.

2.4 Analysis of Spatiotemporal Dynamics

To demonstrate the practical utility of the new R_{rs} dataset for long-term monitoring, we conducted a preliminary spatiotemporal analysis over the study regions. For each pixel and spectral band, a monthly time series of mean R_{rs} was first constructed by averaging all valid retrievals within each calendar month over the 20-year period (i.e., 240 monthly averages per pixel). The overall mean of this time series was then calculated and used to visualize the typical spatial patterns of R_{rs} across the study region.

To detect long-term trends, we applied the seasonal Mann–Kendall test—a non-parametric method that accounts for intra-annual variability and is robust to missing or abnormally distributed data (Mann, 1945; Kendall, 1970)—to the 240-month R_{rs} time series of each pixel. To ensure reliable trend estimation, only pixels with valid data in at least 50% of the months were retained. The rate of change (% yr^{-1}) was then calculated by dividing the Mann–Kendall slope by the corresponding long-term mean R_{rs} for each pixel.

3 Results and Discussion

3.1 *In Situ* Validation

The comprehensive validation (shown in Figure 3) suggested that R_{rs} products generated with the improved processing framework demonstrate strong agreement with field observations across eight MODIS Aqua bands, with data points closely clustered along the 1:1 line. Overall, the average regression slope reaches 1.00 ± 0.08—significantly improved from 0.90 ± 0.06 of the standard products—indicating that the aerosol overcorrection problem in the standard AC was substantially mitigated. The improvement is particularly pronounced in the 488–555 nm range, where our new R_{rs} data consistently outperform the standard products, achieving R^2 values of 0.90±0.02, MdAPE as low as 14.42±1.7%, and NRMSE below 5%. These results confirm that incorporating global gridded aerosol models greatly improves retrieval accuracy in the visible spectrum, which is most relevant to water color applications.

Despite these improvements, some challenges remain in the blue bands (412 and 443 nm), where strong absorption and high aerosol sensitivity complicate AC (Ioccg, 2014; Kirk, 2010). While the regression slopes improve relative to the standard products, other metrics show slightly reduced performance, likely due to the limited temporal resolution of monthly aerosol

https://doi.org/10.5194/essd-2025-438
Preprint. Discussion started: 13 August 2025

models in highly dynamic coastal regions. Nevertheless, the use of geographically informed aerosol priors still helps reduce the overcorrection tendencies typical of the standard products.

In the red bands (667 and 678 nm), a slight overestimation is observed (slopes = 1.06–1.16), possibly due to uncertainties in aerosol absorption assumptions or the inherently low magnitude of R_{rs} signals at these wavelengths (Ioccg, 2019). Even so, our new data better preserves high R_{rs} values in turbid waters, which are often underestimated in the standard product due to conservative assumptions about aerosol absorption.

In summary, the improved processing framework substantially enhances the accuracy of satellite-derived R_{rs}, particularly by improving aerosol correction in optically complex coastal waters through the flexible use of global gridded aerosol models. This improvement ensures more reliable R_{rs} inputs for coastal monitoring, long-term change detection, and ecological modeling.

https://doi.org/10.5194/essd-2025-438
Preprint. Discussion started: 13 August 2025

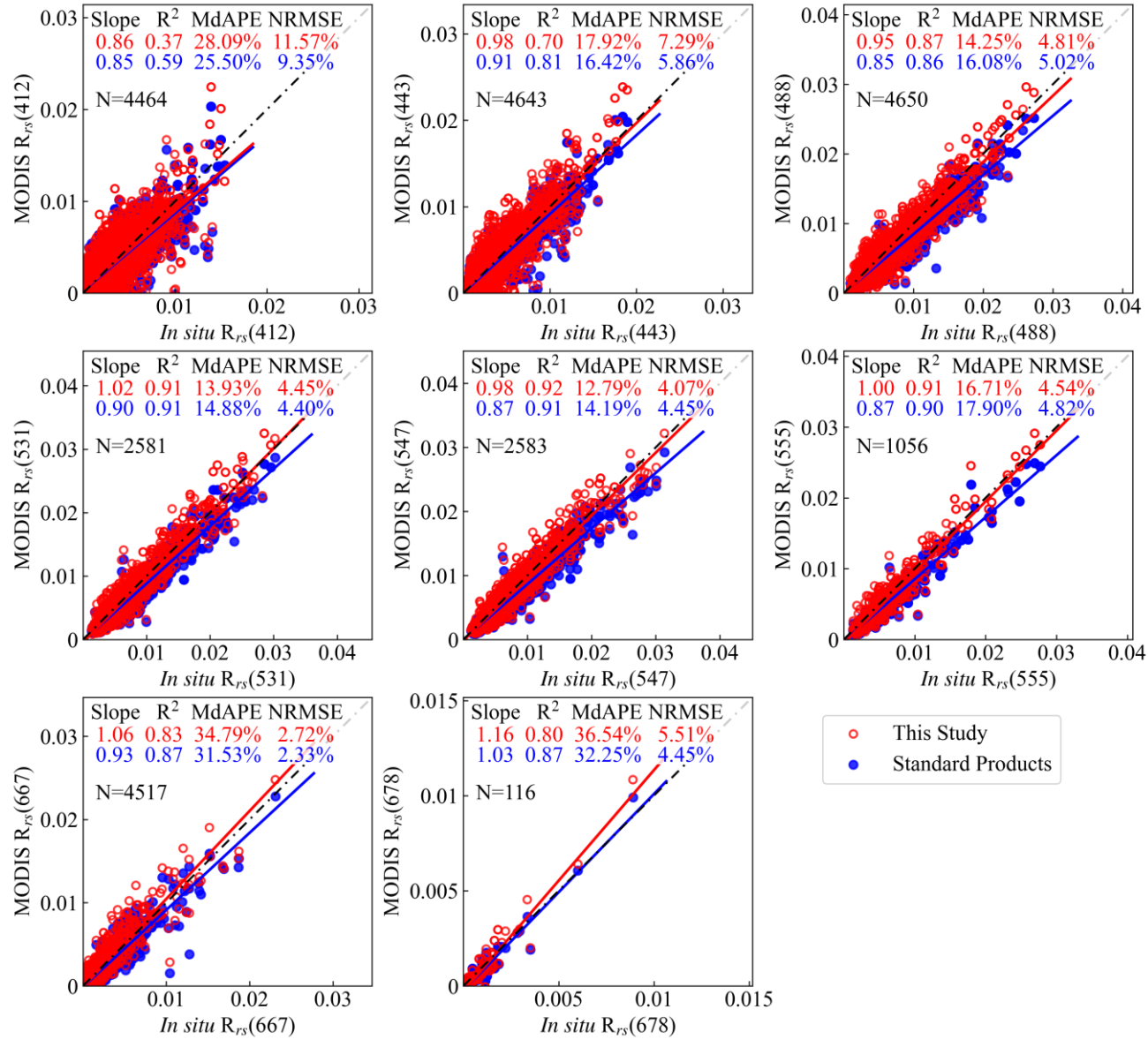

Figure 3: Scatter plots showing the validation of R_{rs} from this study and from NASA standard MODIS Aqua products against *in situ* measurements across eight spectral bands. Accuracy metrics and the number of match-ups (N) are annotated.

3.2 Valid Data Yield Comparison Analysis

Figure 4 presents the spatial distribution of valid observations (VO) at 443 nm for both the new R_{rs} dataset and standard products, along with their difference (VOD), over the coastal waters of China and the US in 2007 (region locations shown in

https://doi.org/10.5194/essd-2025-438
Preprint. Discussion started: 13 August 2025

Figure 1). The year 2007 was selected as a reference due to its high data availability and broad spatial coverage in both study regions, providing a practical basis for consistent comparison.

In the Chinese coastal waters, the new dataset consistently yields more valid retrievals than the standard products, with notable improvements in the Bohai Sea, the Yellow Sea, and along the broader coastline. On average, the new dataset provides 51 VO per pixel per year, with local maxima reaching 140 days in the Bohai Sea—a region where semi-enclosed geography and sediment-laden river inflows result in persistently turbid conditions that challenge conventional AC (Xu et al., 2018). In contrast, the standard products yield an average of 32 VO, with a maximum of ~110 days observed off the northern coast of the Philippines. The resulting VOD indicates an average increase of 18 days per year in the Chinese coastal waters, reaching up to 94 days in some areas. These improvements reflect the enhanced retrieval capacity of the new processing framework in optically complex coastal regions where the standard operational processing tends to underperform.

In the US coastal waters, the difference between the two datasets is generally smaller but still appreciable. The new dataset achieves an average of 80 VO per year, compared to 68 from the standard products. Both datasets report their highest VO in the Gulf of California, with values of 232 (new) and 225 (standard). The average VOD in this region is 12 days per year, with localized peaks up to 115 days, particularly around Chesapeake Bay, the western Gulf of Mexico, and Cuba.

Overall, the new dataset delivers a regional average increase of 18 days per year in the Chinese coastal waters and 12 days per year in the US coastal waters for $R_{rs}(443)$, corresponding to relative gains of approximately 56% and 18%, respectively. Similar improvements are observed at other visible wavelengths, as illustrated in Figures 5 and 6 for 547 nm and 667 nm, further confirming the broader enhancement in valid data yield provided by the new dataset across the visible spectrum.

https://doi.org/10.5194/essd-2025-438
Preprint. Discussion started: 13 August 2025

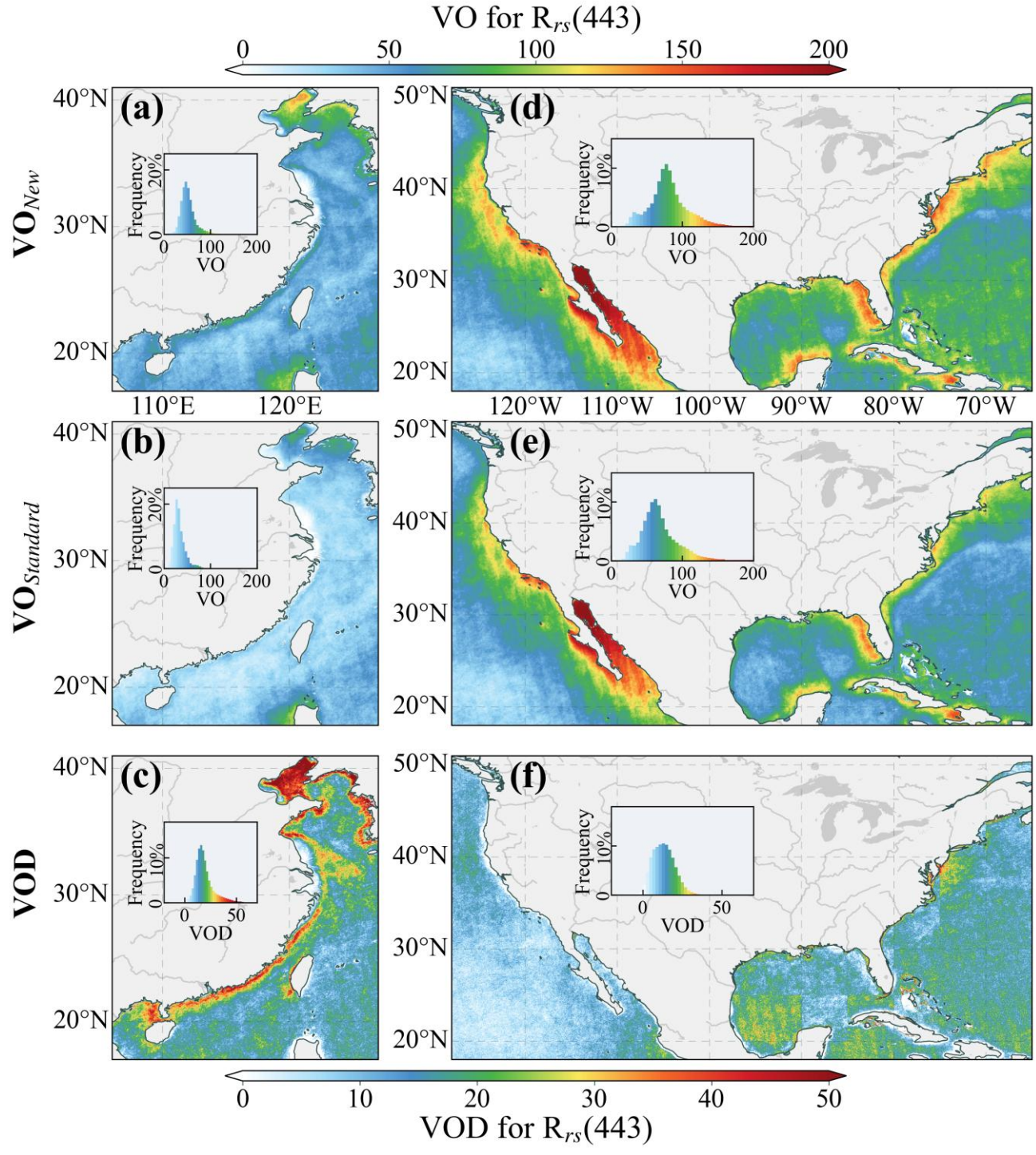

Figure 4: Spatial distribution of valid observations for the new dataset (VO_{New}), the standard products ($VO_{Standard}$) and their difference (VOD, valid observation difference) for R_{rs}(443) in the coastal waters of China and the United States (US) in 2007.

https://doi.org/10.5194/essd-2025-438
Preprint. Discussion started: 13 August 2025

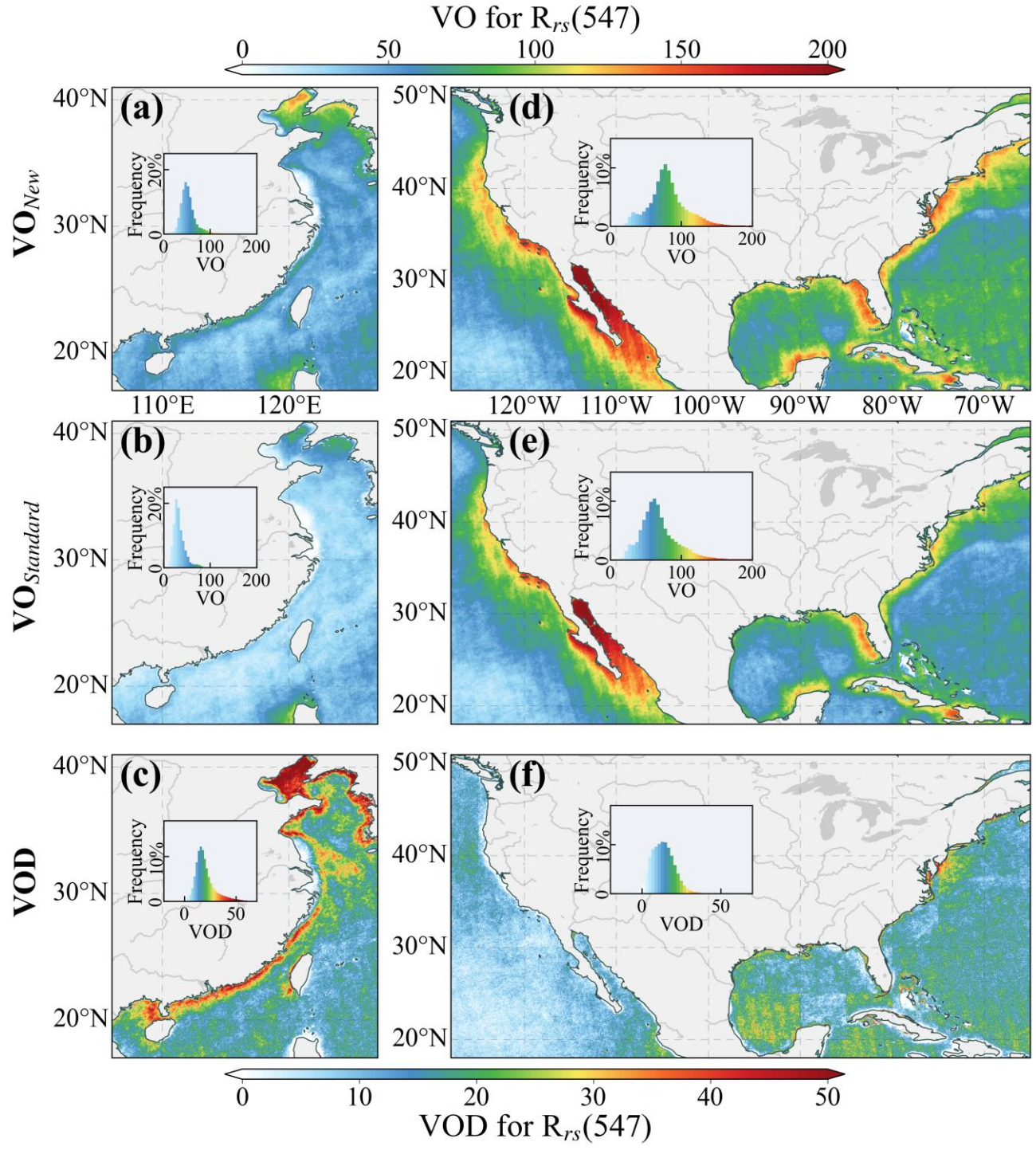

320 **Figure 5: Spatial distribution of VO_{New}, $VO_{Standard}$, and VOD for R_{rs}(547) in the coastal waters of China and the US in 2007.**

https://doi.org/10.5194/essd-2025-438
Preprint. Discussion started: 13 August 2025

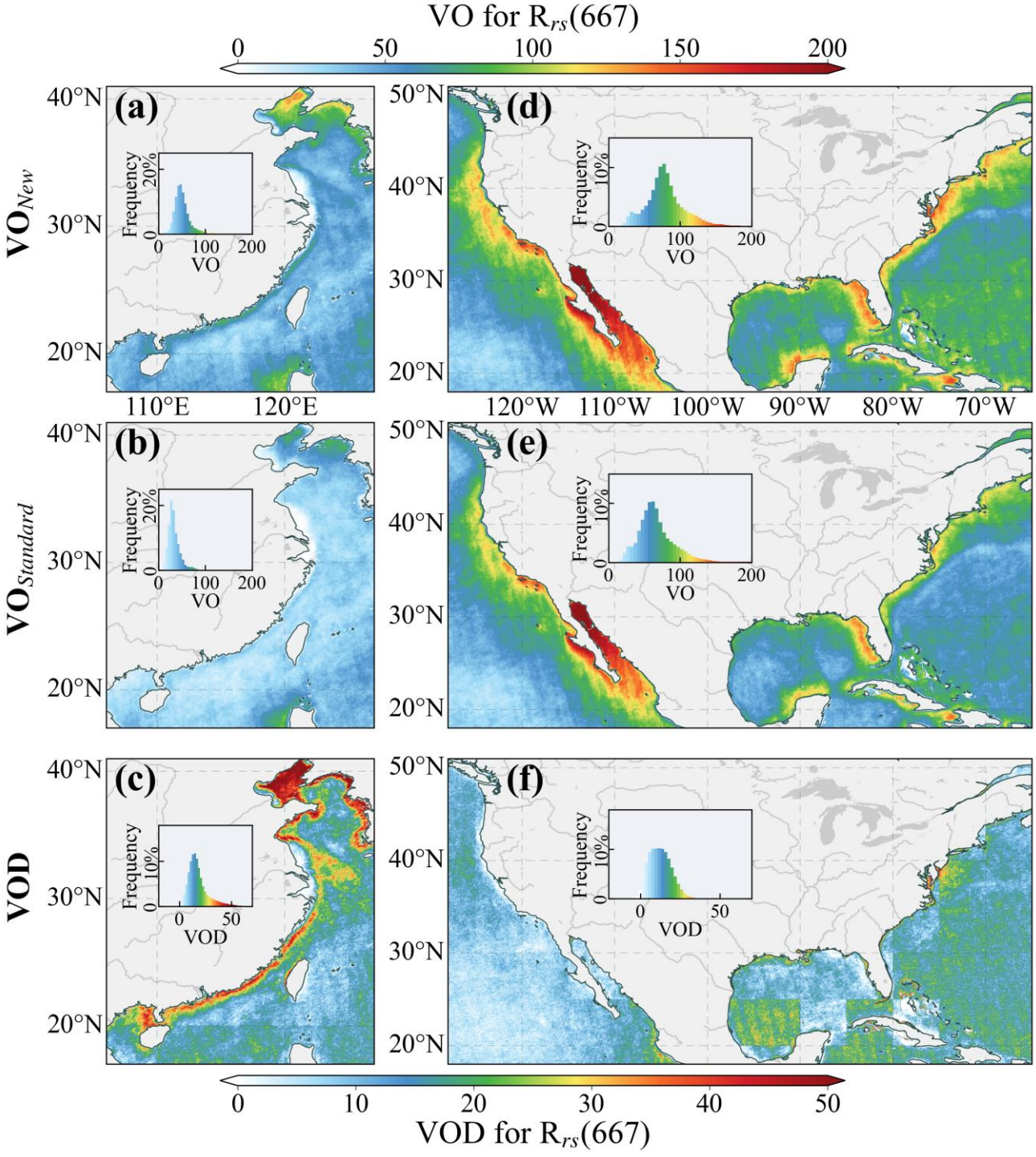

Figure 6: Spatial distribution of VO_{New}, $VO_{Standard}$, and VOD for R_{rs}(667) in the coastal waters of China and the US in 2007.

https://doi.org/10.5194/essd-2025-438
Preprint. Discussion started: 13 August 2025


Open Access Earth System Science Data Discussions

Since cloud masking significantly affects the availability of valid satellite ocean color retrievals (Zhao et al., 2023; Zhang et al., 2014), a sensitivity analysis was conducted to isolate the effect of the updated cloud-masking strategy on data availability.

Specifically, we reprocessed the 2007 MODIS data for both study regions using the standard NIR iterative AC algorithm and the AF10 aerosol models, but replaced the default cloud-masking threshold ($R_{rc,869}$ = 0.027) with the revised threshold ($R_{rc,2130}$ = 0.037) adopted in our processing framework. All other processing steps, including the QC procedures described in Sect. 2.2.2, were kept consistent. The resulting VO under this configuration is denoted as $VO_{AF10\&2130}$, which was then compared to the new dataset's VO_{New}. Their difference, defined as $VOD_{AF10\&2130} = VO_{New} - VO_{AF10\&2130}$, quantifies the change of VO when using the full improved framework beyond the cloud-masking update alone.

Results show that adjusting the cloud-masking threshold alone leads to substantial increases in VO relative to the standard products ($VO_{AF10\&2130} > VO_{Standard}$ in Figure 4), particularly along the Chinese coast. This confirms that the updated threshold more effectively preserves valid water pixels in highly turbid areas that would otherwise be incorrectly excluded.

Interestingly, Figure 7 shows that $VOD_{AF10\&2130}$ is negative in many regions, suggesting that the AF10&2130 configuration can sometimes produce more VO than our full processing framework. However, the added retrievals may not be of comparable quality. Although these additional pixels passed the same QC filters, these filters—especially those based on spectral shape and signal saturation—were optimized for the improved processing framework. Consequently, they may not fully capture retrieval errors specific to the AF10&2130 configuration, especially the known R_{rs} underestimation issue associated with AF10 models in coastal waters (see Figure 3).

Overall, the new dataset achieves a more balanced outcome by integrating a spatially adaptive aerosol model selection strategy, an improved cloud mask, and tailored QC criteria. These components jointly enhance not only the data yield but also the reliability of R_{rs} retrievals in challenging coastal environments.

https://doi.org/10.5194/essd-2025-438
Preprint. Discussion started: 13 August 2025

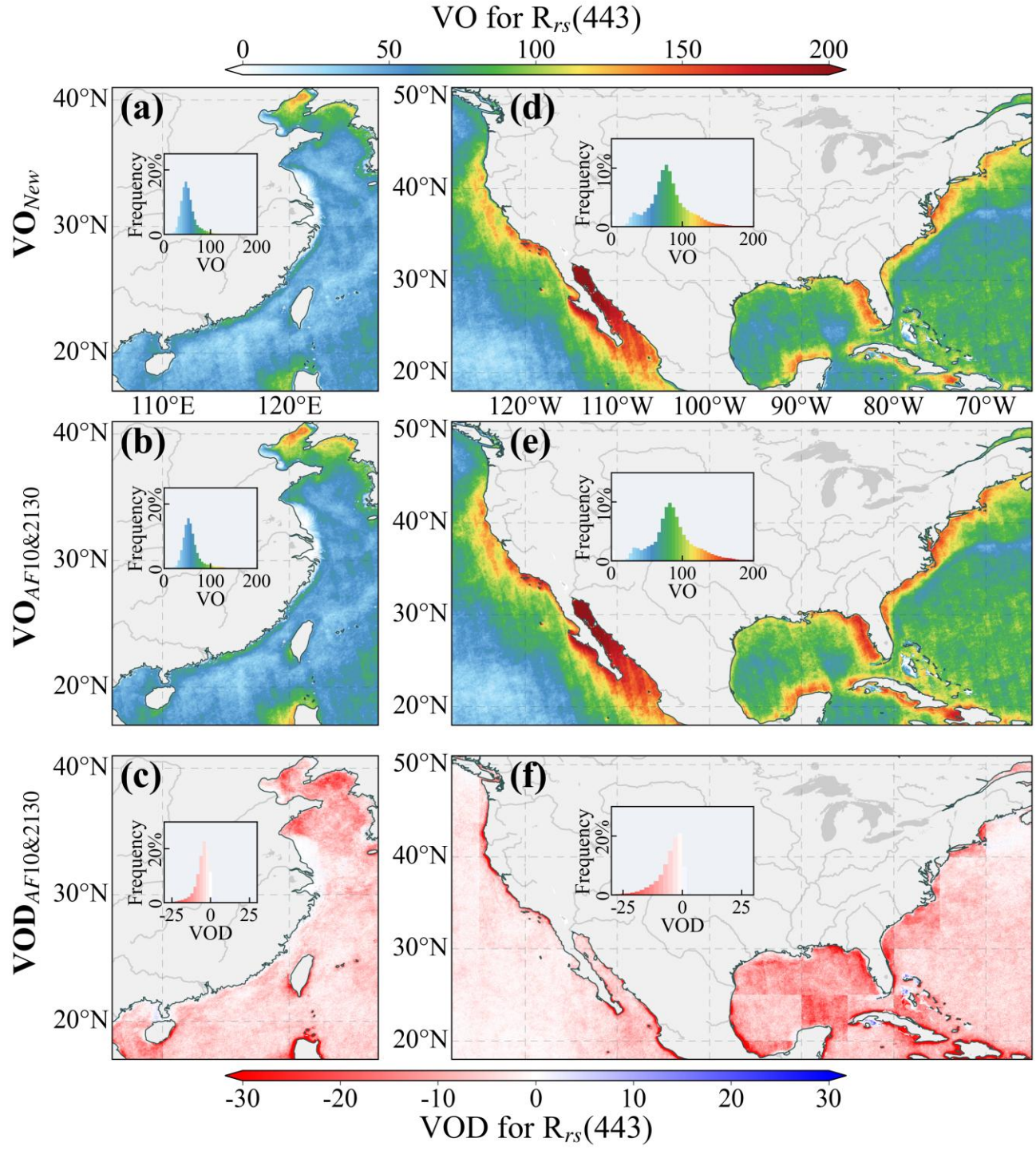

Figure 7: Spatial distribution of valid observations for the new dataset (VO_{New}), the AF10&2130 configuration ($VO_{AF10\&2130}$) and their difference ($VOD_{AF10\&2130} = VO_{New} - VO_{AF10\&2130}$) for R_{rs}(443) in the coastal waters of China and the US in 2007.

https://doi.org/10.5194/essd-2025-438
Preprint. Discussion started: 13 August 2025

3.3 Single-Scene Imagery Comparison

To further assess the utility of the new R_{rs} dataset, we conducted single-scene comparisons across four representative coastal regions: the Pearl River Estuary, the Bohai Sea, the Chesapeake Bay, and the Mississippi Estuary (see Figure 1 for their locations). This analysis aimed to evaluate the dataset's ability to capture regional R_{rs} features under diverse optical conditions.

Figure 8 presents the results for the Pearl River Estuary and the Bohai Sea, both characterized by turbid nearshore waters (Liu et al., 2012; Xu et al., 2018). While both datasets broadly reproduce the spatial patterns of R_{rs}, the new dataset provides markedly more extensive valid data coverage. For instance, the standard products yield few to no valid pixels within the Pearl River Estuary and large portions of the Bohai Sea, whereas the new dataset successfully retrieves R_{rs} values in these areas.

The QC mask analysis reveals that most of the missing values in the standard products are flagged as cloud- or ice-contaminated. In contrast, the successful retrievals in the new dataset suggest that these regions are actually cloud-free but exhibit high reflectance due to intense turbidity, leading to misclassification by the standard cloud mask. By adopting a revised cloud mask threshold and aerosol models better suited to turbid conditions, the new dataset retains a greater number of valid pixels, thereby enabling a more complete and accurate depiction of regional R_{rs} patterns. For example, in the western nearshore region of the Pearl River Estuary, the new dataset reveals a distinct high-reflectance band likely associated with suspended sediments along the coast—a feature entirely absent in the standard products due to cloud misclassification. This highlights the improved capability of the new dataset to preserve fine-scale coastal structures that are frequently lost under conventional processing.

Notably, further inspection of the QC masks reveals that, in addition to improved retention of valid water pixels through the updated cloud mask, some pixels—though not flagged as clouds—were still excluded by the "Wrong Turbid Water Mask" and "Saturated $R_{rs}(667)$ Mask" (i.e., the spectral-shape and saturation-based QC filters introduced in Sect. 2.2.2). This suggests that the newly implemented QC filters play a complementary role to cloud masking by identifying additional suspect pixels—such as those with atypical spectral shapes or signal saturation—that might otherwise be retained. This added filtering helps enhance the overall reliability of the retained R_{rs} data.

In addition to enhanced coverage, the new dataset also exhibits slightly higher R_{rs} values at identical locations. For instance, in the Pearl River Estuary, the average $R_{rs}(547)$ in the sample window (indicated by black rectangles in Figure 8; the same symbol is used for other sample windows below) increases from approximately 0.0227 to 0.0239 sr^{-1}; in Bohai Bay, the value rises from 0.0213 to 0.0244 sr^{-1}. These differences underscore the improved retrieval capability of the improved processing framework, particularly in mitigating the underestimation tendency associated with AF10 models (as also evidenced in Figure 3).

https://doi.org/10.5194/essd-2025-438
Preprint. Discussion started: 13 August 2025

Nevertheless, the new dataset still fails to retrieve valid data in extremely turbid zones, such as parts of the western Bohai Sea, pointing to remaining challenges in processing waters with extremely high reflectance.

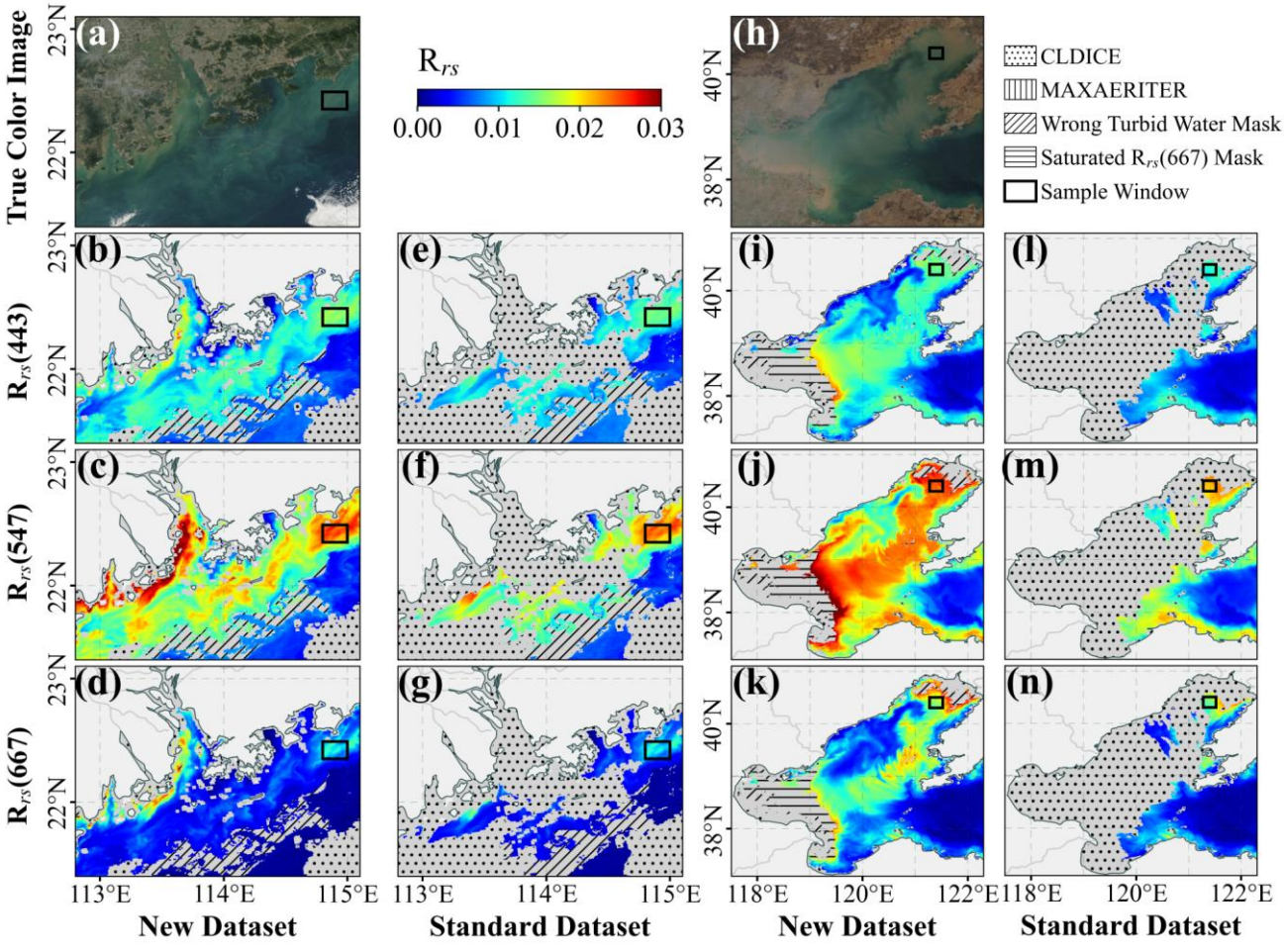

Figure 8: Comparison of R_{rs} (units: sr^{-1}) derived from single-scene MODIS Aqua observations over the Pearl River Estuary (2014-12-14) and Bohai Sea (2020-03-11). For each region, the top image shows a true color composite (panels a and h), followed by R_{rs} at 443, 547, and 667 nm from the new dataset (panels b–d and i–k) and from the standard dataset (panels e–g and l–n), respectively. Invalid pixels are marked with hatched patterns based on quality control masks. Black rectangles indicate sample windows used for regional comparison.

We further examined two representative regions in the US coastal waters: the Chesapeake Bay and the Mississippi Estuary. As shown in Figure 9, both datasets reveal generally consistent spatial distributions of R_{rs}, supporting the reliability of the new dataset. However, clear differences in data availability are observed. True color composite combined with mask analysis

https://doi.org/10.5194/essd-2025-438
Preprint. Discussion started: 13 August 2025

reveals that the new dataset exhibits greater resistance to thin cloud contamination, allowing successful retrievals over pixels that are missing in the standard products, such as those in the northern Chesapeake Bay and western Mississippi River Delta. The relaxed cloud mask helps preserve these pixels, while the adoption of more appropriate aerosol models enables more accurate retrievals rather than underestimation. Within the highlighted sample windows, the new dataset also yields slightly elevated R_{rs} values—for example, approximately 0.0113 sr^{-1} vs. 0.0097 sr^{-1} in the Chesapeake Bay, and 0.0169 sr^{-1} vs. 0.0156 sr^{-1} in the Mississippi Estuary—further indicating improved performance in mitigating overcorrection caused by the AF10 models. These results suggest that the observed improvements are not region-specific but hold across geographically and optically diverse coastal waters.

https://doi.org/10.5194/essd-2025-438
Preprint. Discussion started: 13 August 2025

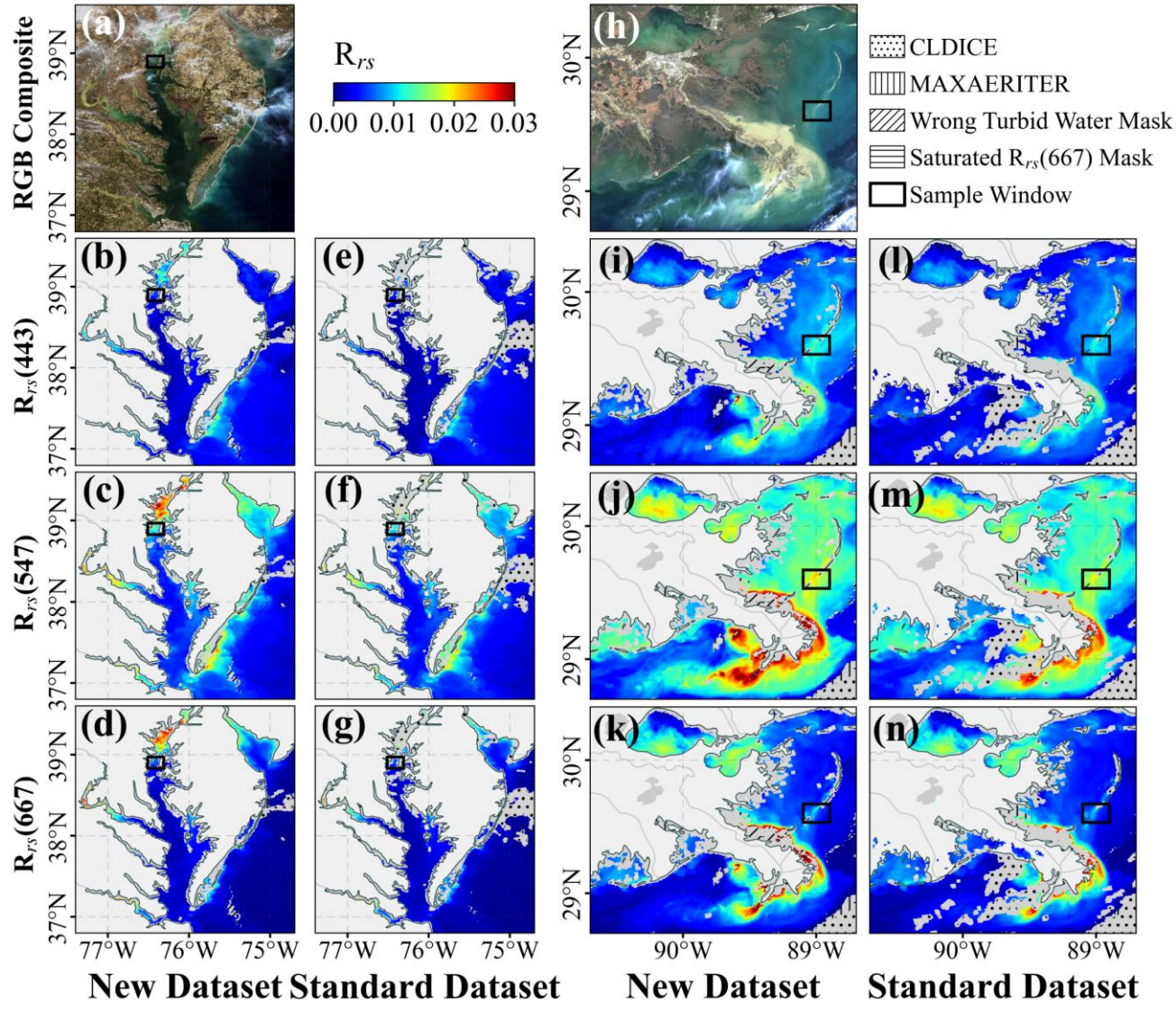

Figure 9: Comparison of R_{rs} (units: sr^{-1}) derived from single-scene MODIS Aqua observations over the Chesapeake Bay (2019-02-05) and the Mississippi Estuary (2021-01-13). For each region, the top image shows a true color composite (panels a and h), followed by R_{rs} at 443, 547, 667 nm from the new dataset (panels b–d and i–k) and from the standard dataset (panels e–g and l–n), respectively. Invalid pixels are marked with hatched patterns based on quality control masks. Black rectangles indicate sample windows used for regional comparison.

In summary, the new dataset demonstrates superior performance in preserving valid retrievals and accurately capturing subtle gradients across optically complex coastal waters. These improvements enhance its suitability for detailed ocean color analysis and reliable assessment of water quality in challenging nearshore environments.

https://doi.org/10.5194/essd-2025-438
Preprint. Discussion started: 13 August 2025

3.4 Spatiotemporal Patterns and Trends

Figure 10 illustrates the spatial distribution of long-term mean R_{rs} values at 443, 547, and 667 nm for the coastal waters of China and the US over the 2003-2022 period. These patterns reveal clear wavelength dependence and regional variability.

In Chinese coastal waters (Figures 10a–c), the regional average $R_{rs}(443)$ is 0.00679 sr^{-1}, rising to 0.00866 sr^{-1} within the 30 m isobath (marked by the white dashed line), where optically complex conditions dominate. Notably high $R_{rs}(443)$ values are observed in nearshore areas such as the western Bohai Sea (0.00738 sr^{-1}), the Yangtze River Estuary and Hangzhou Bay (0.01213 sr^{-1}), the Pearl River Estuary, and the eastern Beibu Gulf. These high $R_{rs}(443)$ values persist despite strong absorption by high concentrations of CDOM and Chl, suggesting that backscattering by suspended sediments dominates the blue reflectance signal in these turbid waters (Kirk, 2010; Feng et al., 2014; Ye et al., 2016). In contrast, significantly low $R_{rs}(443)$ values (<0.003 sr^{-1}) occur in the central and northern Yellow Sea, where sediment loads are reduced and absorption remains high, resulting in suppressed reflectance in the blue band (Kirk, 2010; Ye et al., 2016; Ling et al., 2020). At longer wavelengths (547 and 667 nm), high R_{rs} values are more restricted to highly turbid nearshore and estuarine waters. Within the 30 m isobath, the mean $R_{rs}(547)$ and $R_{rs}(667)$ values reach 0.01551 sr^{-1} and 0.00819 sr^{-1}, respectively, decreasing to 0.00506 sr^{-1} and 0.00184 sr^{-1} farther offshore. These spatial patterns reflect the varying contributions of optically active constituents to spectral reflectance.

In US coastal waters (Figures 10d–f) the long-term mean R_{rs} values exhibit distinct spatial features. At 443 nm, high R_{rs} values (>0.03 sr^{-1}) are found around the shallow Bahamas Banks, while low values (<0.003 sr^{-1}) dominate the East and West Coasts of the US, indicative of strong absorption by CDOM and Chl (Mannino et al., 2008; Kirk, 2010). At 547 nm and 667 nm, high R_{rs} values are observed in regions such as the northwestern Gulf of California, the Gulf of Mexico coast, and around Chesapeake Bay. As in the Chinese coastal waters, R_{rs} decreases sharply with increasing distance from shore.

https://doi.org/10.5194/essd-2025-438
Preprint. Discussion started: 13 August 2025

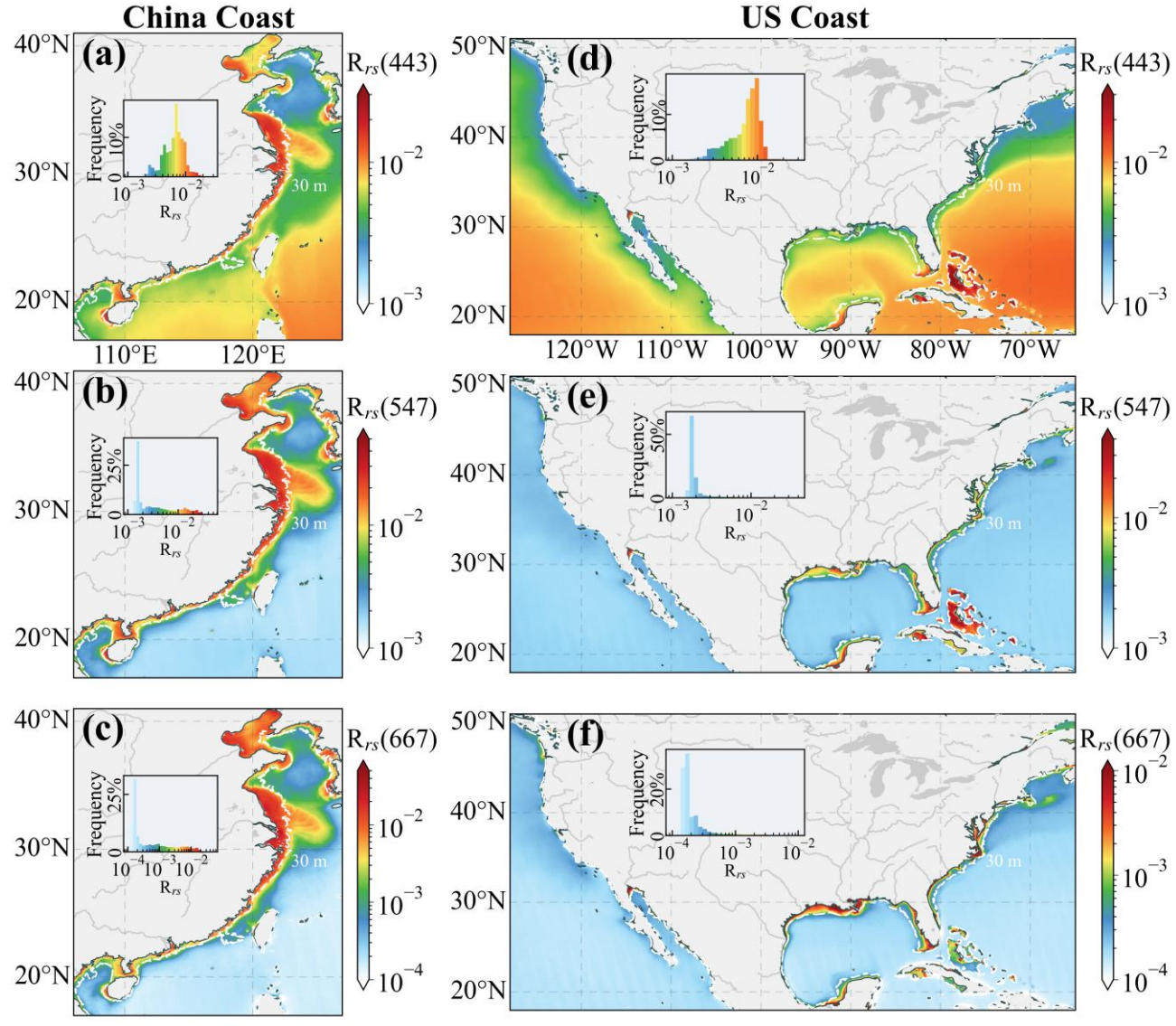

Figure 10: Spatial distribution of long-term mean R_{rs} (units: sr^{-1}) at 443, 547, and 667 nm for China (a – c) and US (d – f) coastal waters, derived from the new dataset (2003-2022). White dashed lines indicate the approximate 30 m isobath.

435 Figure 11 illustrates the spatial distribution of long-term R_{rs} trends (% yr^{-1}) for the same wavelengths, as estimated using the seasonal Mann-Kendall test over the 240-month period.

In Chinese coastal waters (Figures 11a–c), $R_{rs}(443)$ generally shows increasing trends, with a mean rate of 0.64% yr^{-1} and localized peaks reaching 6.85% yr^{-1} in the central Yellow Sea. $R_{rs}(547)$ and $R_{rs}(667)$ also exhibit upward trends in this region, potentially reflecting rising suspended sediment concentrations and declining Chl and CDOM levels in recent years, as

https://doi.org/10.5194/essd-2025-438
Preprint. Discussion started: 13 August 2025

previously observed by Wang et al. (2023). In contrast, most of Laizhou Bay, Bohai Bay, and the eastern Liaodong Bay show consistent negative trends across all three wavelengths, possibly indicating a reduction in suspended sediment loads. This trend aligns with earlier findings that attribute such declines to weakening wind-driven sediment resuspension (Li et al., 2022; Zhao et al., 2022). The mean trends for $R_{rs}(547)$ and $R_{rs}(667)$ are 0.18% yr^{-1} and 0.24% yr^{-1}, respectively, although widespread declines are also evident in other areas, such as the northern South China Sea, with maximum decreases reaching -6.70% yr^{-1} and -9.08% yr^{-1}.

In the US coastal waters (Figures 11d–f), $R_{rs}(443)$ exhibits a mean increase of 0.28% yr^{-1}, with peak increases reaching 7.22% yr^{-1}, Strong positive trends are observed along the US West Coast, near the Bahamas, and within the Gulf Stream region. In contrast, notable declines occur in areas such as southern Florida Peninsula and the western Gulf of Mexico, with rates reaching -6.06% yr^{-1}. For $R_{rs}(547)$ and $R_{rs}(667)$, the overall trends are slightly negative (-0.004% yr^{-1} and 0.042% yr^{-1}, respectively), with most coastal regions—except the western Gulf of Mexico—showing decreasing trends, with minimum values of -5.68% yr^{-1} and -7.51% yr^{-1}, respectively. A particularly complex pattern emerges along the Gulf Stream: while $R_{rs}(443)$ increases significantly, $R_{rs}(547)$ and $R_{rs}(667)$ exhibit moderate decreases. This may reflect the growing influence of oligotrophic Gulf Stream waters (Leonelli et al., 2022) and enhanced upper-ocean stratification associated with regional ocean warming (Todd and Ren, 2023). These processes are known to suppress vertical mixing and nutrient supply (Li et al., 2020), leading to reduced phytoplankton biomass (Yu et al., 2023) and lower concentrations of suspended matter (Wei et al., 2021) in the surface layer. Such reductions in optically active constituents diminish absorption in the blue bands and scattering in the green and red bands, consistent with the observed R_{rs} trends in this region. Additionally, the magnitude of R_{rs} trends is greater in the Chinese coastal waters than in the US coastal waters, likely reflecting stronger anthropogenic influences, hydrological variability, and regional-specific geomorphological settings.

The observed spatiotemporal patterns and trends in R_{rs} underscore the robustness of the new dataset in capturing diverse coastal optical dynamics. Their consistency with previously reported trends lends further confidence in the dataset's reliability and demonstrates its value as a foundation for future research into long-term environmental change, human impacts, and climate-related ecosystem responses in coastal waters.

https://doi.org/10.5194/essd-2025-438
Preprint. Discussion started: 13 August 2025

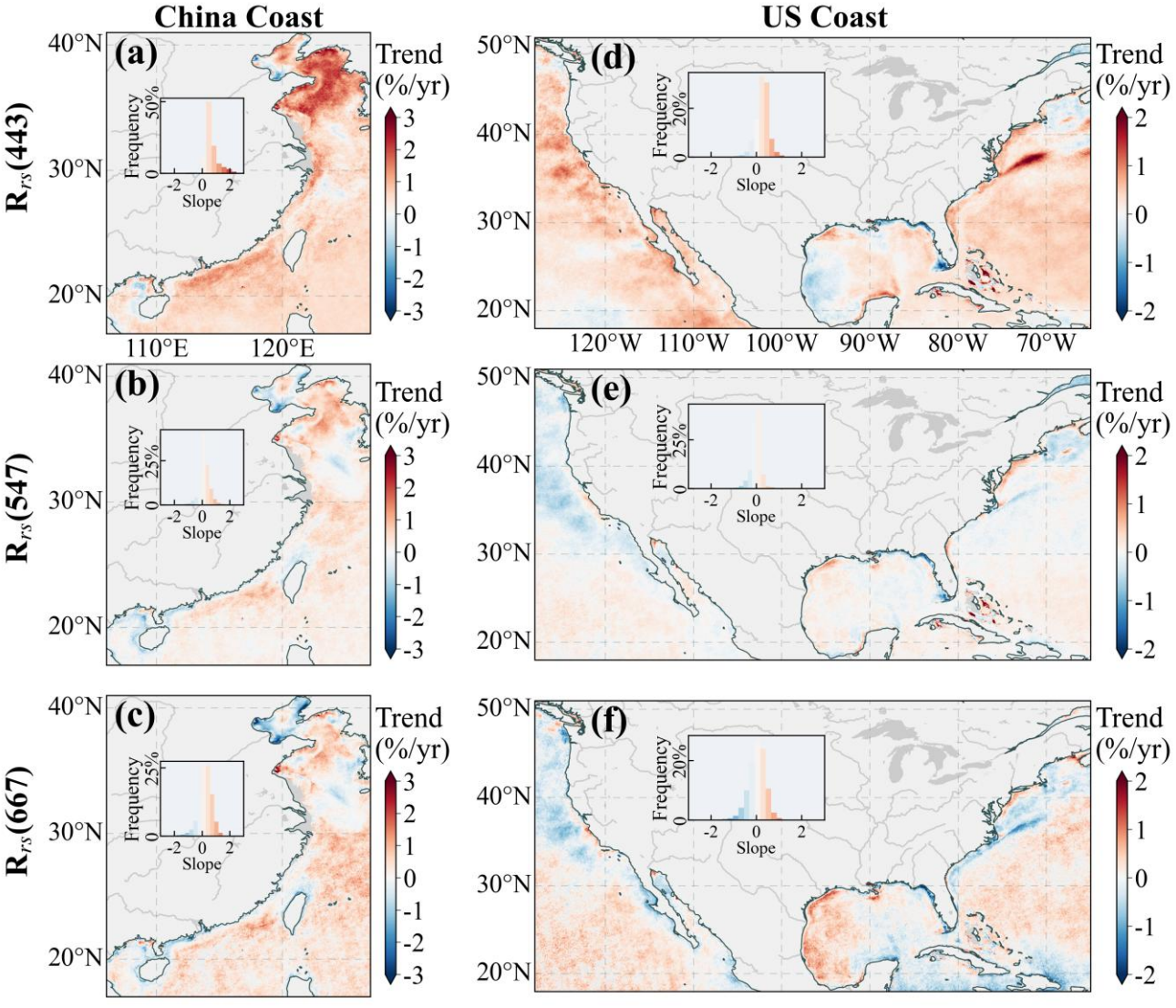

Figure 11: Long-term R_{rs} trends (units: % yr^{-1}) from 2003 to 2022, derived using the seasonal Mann-Kendall test at 443, 547, and 667 nm for China (a – c) and US (d – f) coastal waters. Rates are computed as the Mann-Kendall slope divided by the corresponding 20-year average R_{rs}.

4 Data availability

The high-quality coastal R_{rs} dataset generated in this study is publicly available at https://doi.org/10.5281/zenodo.16413443 (Zhao et al., 2025). The dataset is provided in monthly composites and stored in GeoTIFF format at 0.01° spatial resolution under the EPSG:4326 (WGS84) spatial reference system.

https://doi.org/10.5194/essd-2025-438
Preprint. Discussion started: 13 August 2025

5 Conclusion

This study developed an improved processing framework suitable for coastal waters by integrating previous advancements in aerosol models and cloud masking strategies. A key innovation lies in the implementation of a spatially adaptive aerosol model selection mechanism, which dynamically assigns models based on pixel-level probabilities of continental aerosol influence. In addition, the framework incorporates targeted masking strategies tailored to both possible residual cloud contamination—due to the modified cloud masking threshold—and the occurrence of extreme turbid waters. Using this framework, we generated a high-quality R_{rs} dataset from MODIS Aqua observations for the coastal waters of China and the United States from 2003 to 2022. The resulting dataset was rigorously evaluated against the NASA standard R_{rs} products through a series of comparative analyses under consistent and stringent quality control strategies.

Compared to standard products, products generated with the improved processing framework exhibit substantial enhancements in both retrieval accuracy and valid retrieval coverage, particularly in turbid regions where conventional AC approaches often suffer from overcorrection and cloud misclassification. These enhancements are evident across both pixel-level validations and large-scale analyses, demonstrating the new dataset's improved ability to preserve valid water-leaving signals and resolve fine-scale coastal features. The revealed spatiotemporal patterns and long-term trends of R_{rs} further underscore the new dataset's capability to characterize coastal optical variability, supporting its application in long-term monitoring, water quality assessment, and environmental change studies.

Although this study focused on MODIS Aqua and two regional case studies, the methodology is scalable and transferable to other sensors and global coastal zones. Future work may involve broader *in situ* validation and the application of this dataset to retrieve biogeochemical parameters such as Chl, suspended sediments, and CDOM, thereby extending its utility for coastal management and climate-related research.

6 Author contributions

JL, YW and SZ developed and implemented the improved atmospheric correction algorithm. YW and SZ designed quality control strategies. JL and SZ collected and processed the data. SZ analyzed the data and wrote the paper. DZ provided refined aerosol models. YZ helped refine the scientific question. LF conceptualized the study and designed the research framework. All of the co-authors revised the paper.

7 Competing interests

The contact author has declared that none of the authors has any competing interests.

https://doi.org/10.5194/essd-2025-438
Preprint. Discussion started: 13 August 2025

References

Ahmad, Z., Franz, B. A., McClain, C. R., Kwiatkowska, E. J., Werdell, J., Shettle, E. P., and Holben, B. N.: New aerosol models for the retrieval of aerosol optical thickness and normalized water-leaving radiances from the SeaWiFS and MODIS sensors over coastal regions and open oceans, Appl. Opt., 49, 5545-5560, 10.1364/AO.49.005545, 2010.

Bailey, S. W. and Werdell, P. J.: A multi-sensor approach for the on-orbit validation of ocean color satellite data products, Remote Sensing of Environment, 102, 12-23, https://doi.org/10.1016/j.rse.2006.01.015, 2006.

Bassani, C., Manzo, C., Braga, F., Bresciani, M., Giardino, C., and Alberotanza, L.: The impact of the microphysical properties of aerosol on the atmospheric correction of hyperspectral data in coastal waters, Atmos. Meas. Tech., 8, 1593-1604, 10.5194/amt-8-1593-2015, 2015.

Bru, D., Lubac, B., Normandin, C., Robinet, A., Leconte, M., Hagolle, O., Martiny, N., and Jamet, C.: Atmospheric Correction of Multi-Spectral Littoral Images Using a PHOTONS/AERONET-Based Regional Aerosol Model, https://doi.org/10.3390/rs9080814, 2017.

Charlson, R. J., Schwartz, S. E., Hales, J. M., Cess, R. D., Coakley, J. A., Hansen, J. E., and Hofmann, D. J.: Climate Forcing by Anthropogenic Aerosols, Science, 255, 423-430, 1992.

Feng, L., Hu, C., Chen, X., and Song, Q.: Influence of the Three Gorges Dam on total suspended matters in the Yangtze Estuary and its adjacent coastal waters: Observations from MODIS, Remote Sensing of Environment, 140, 779-788, https://doi.org/10.1016/j.rse.2013.10.002, 2014.

Giles, D. M., Holben, B. N., Eck, T. F., Sinyuk, A., Smirnov, A., Slutsker, I., Dickerson, R. R., Thompson, A. M., and Schafer, J. S.: An analysis of AERONET aerosol absorption properties and classifications representative of aerosol source regions, Journal of Geophysical Research: Atmospheres, 117, https://doi.org/10.1029/2012JD018127, 2012.

Gordon, H. R.: Atmospheric correction of ocean color imagery in the Earth Observing System era, Journal of Geophysical Research: Atmospheres, 102, 17081-17106, https://doi.org/10.1029/96JD02443, 1997.

Gordon, H. R. and Wang, M.: Retrieval of water-leaving radiance and aerosol optical thickness over the oceans with SeaWiFS: a preliminary algorithm, Appl. Opt., 33, 443-452, 10.1364/AO.33.000443, 1994.

Gordon, H. R., Du, T., and Zhang, T.: Remote sensing of ocean color and aerosol properties: resolving the issue of aerosol absorption, Appl. Opt., 36, 8670-8684, 10.1364/AO.36.008670, 1997.

Hamill, P., Giordano, M., Ward, C., Giles, D., and Holben, B.: An AERONET-based aerosol classification using the Mahalanobis distance, Atmospheric Environment, 140, 213-233, https://doi.org/10.1016/j.atmosenv.2016.06.002, 2016.

He, X. Q., Pan, D. L., Bai, Y., Zhu, Q. K., and Gong, F.: Evaluation of the aerosol models for SeaWiFS and MODIS by AERONET data over open oceans, Appl. Opt., 50, 4353-4364, 10.1364/AO.50.004353, 2011.

Hu, C., Feng, L., Lee, Z., Davis, C. O., Mannino, A., McClain, C. R., and Franz, B. A.: Dynamic range and sensitivity requirements of satellite ocean color sensors: learning from the past, Appl. Opt., 51, 6045-6062, 10.1364/AO.51.006045, 2012.

Hu, C., Feng, L., Lee, Z., Franz, B. A., Bailey, S. W., Werdell, P. J., and Proctor, C. W.: Improving Satellite Global Chlorophyll a Data Products Through Algorithm Refinement and Data Recovery, Journal of Geophysical Research: Oceans, 124, 1524-1543, https://doi.org/10.1029/2019JC014941, 2019.

Husar, R. B., Prospero, J. M., and Stowe, L. L.: Characterization of tropospheric aerosols over the oceans with the NOAA advanced very high resolution radiometer optical thickness operational product, Journal of Geophysical Research: Atmospheres, 102, 16889-16909, https://doi.org/10.1029/96JD04009, 1997.

IOCCG, Wang, M. (Ed.): Atmospheric Correction for Remotely-Sensed Ocean-Colour Products, Reports of the International Ocean Colour Coordinating Group, IOCCG, Dartmouth, Canada2010.

https://doi.org/10.5194/essd-2025-438
Preprint. Discussion started: 13 August 2025

IOCCG, Sathyendranath, S. (Ed.): Phytoplankton Functional Types from Space, Reports of the International Ocean Colour Coordinating Group, IOCCG, Dartmouth, Canada2014.

IOCCG, Mlin, F. (Ed.): Uncertainties in Ocean Colour Remote Sensing, Reports of the International Ocean Colour Coordinating Group, IOCCG, Dartmouth, Canada2019.

Kendall, M. G.: Rank Correlation Methods, 4th, Griffin1970.

Kirk, J. T. O.: Light and Photosynthesis in Aquatic Ecosystems, 3, Cambridge University Press, Cambridge, DOI: 10.1017/CBO9781139168212, 2010.

Lee, Z., Carder, K. L., and Arnone, R. A.: Deriving inherent optical properties from water color: a multiband quasi-analytical algorithm for optically deep waters, Appl. Opt., 41, 5755-5772, 10.1364/AO.41.005755, 2002.

Leonelli, F. E., Bellacicco, M., Pitarch, J., Organelli, E., Buongiorno Nardelli, B., de Toma, V., Cammarota, C., Marullo, S., and Santoleri, R.: Ultra-Oligotrophic Waters Expansion in the North Atlantic Subtropical Gyre Revealed by 21 Years of Satellite Observations, Geophysical Research Letters, 49, e2021GL096965, https://doi.org/10.1029/2021GL096965, 2022.

Li, G., Cheng, L., Zhu, J., Trenberth, K. E., Mann, M. E., and Abraham, J. P.: Increasing ocean stratification over the past half-century, Nature Climate Change, 10, 1116-1123, 10.1038/s41558-020-00918-2, 2020.

Li, P., Chen, S., Ke, Y., Ji, H., Li, P., and Fan, Y.: Spatiotemporal dynamics of suspended particulate matter in the Bohai Sea, China over the past decade from the space perspective, Science of The Total Environment, 851, 158210, https://doi.org/10.1016/j.scitotenv.2022.158210, 2022.

Ling, Z., Sun, D., Wang, S., Qiu, Z., Huan, Y., Mao, Z., and He, Y.: Remote sensing estimation of colored dissolved organic matter (CDOM) from GOCI measurements in the Bohai Sea and Yellow Sea, Environmental Science and Pollution Research, 27, 6872-6885, 10.1007/s11356-019-07435-6, 2020.

Liu, J., Yan, W., Chen, Z., and Lu, J.: Sediment sources and their contribution along northern coast of the South China Sea: Evidence from clay minerals of surface sediments, Continental Shelf Research, 47, 156-164, https://doi.org/10.1016/j.csr.2012.07.013, 2012.

Lv, J., Feng, L., and Zhao, D.: Validation of Global Gridded Aerosol Models in Inland/Coastal Water Atmospheric Correction for MODIS, VIIRS, and Landsat, IEEE Transactions on Geoscience and Remote Sensing, 62, 1-10, 10.1109/TGRS.2024.3427836, 2024.

Mann, H. B.: Nonparametric Tests Against Trend, Econometrica, 13, 245-259, 10.2307/1907187, 1945.

Mannino, A., Russ, M. E., and Hooker, S. B.: Algorithm development and validation for satellite-derived distributions of DOC and CDOM in the U.S. Middle Atlantic Bight, Journal of Geophysical Research: Oceans, 113, https://doi.org/10.1029/2007JC004493, 2008.

Mélin, F., Zibordi, G., and Holben, B. N.: Assessment of the Aerosol Products From the SeaWiFS and MODIS Ocean-Color Missions, IEEE Geoscience and Remote Sensing Letters, 10, 1185-1189, 10.1109/LGRS.2012.2235408, 2013.

Mobley, C., Werdell, J., Franz, B., Ahmad, Z., and Bailey, S.: Atmospheric Correction for Satellite Ocean Color Radiometry, 10.13140/RG.2.2.23016.78081, 2016.

Montes, M., Pahlevan, N., Giles, D. M., Roger, J.-C., Zhai, P.-w., Smith, B., Levy, R., Werdell, P. J., and Smirnov, A.: Augmenting Heritage Ocean-Color Aerosol Models for Enhanced Remote Sensing of Inland and Nearshore Coastal Waters, Frontiers in Remote Sensing, 3, 2022.

Ancillary Data Sources: https://oceancolor.gsfc.nasa.gov/resources/docs/ancillary/, last access: 2024-11-04.

NASA Ocean Biology Processing Group: Aqua MODIS Level-2 Regional Ocean Color (OC) Data (version 2022.0), NASA Ocean Biology Distributed Active Archive Center [dataset], 10.5067/AQUA/MODIS/L2/OC/2022.0, 2022.

MODIS Data Degradation Notice: https://forum.earthdata.nasa.gov/viewtopic.php?t=5333, last access: 2025-07-03.

https://doi.org/10.5194/essd-2025-438
Preprint. Discussion started: 13 August 2025

O'Reilly, J.: Ocean color chlorophyll a algorithms for SeaWiFS, OC2, and OC4: Version 4, SeaWiFS Postlaunch Calibration and Validation Analyses, 11, 9-23, 2000.

Prospero, J. M., Charlson, R. J., Mohnen, V., Jaenicke, R., Delany, A. C., Moyers, J., Zoller, W., and Rahn, K.: The atmospheric aerosol system: An overview, Reviews of Geophysics, 21, 1607-1629, https://doi.org/10.1029/RG021i007p01607, 1983.

Robinson, W., Franz, B., Patt, F., Bailey, S., and Werdell, J.: Masks and flags updates, NASA Technical Memorandum - SeaWIFS Postlaunch Technical Report Series, 34-40, 2003.

Shettle, E. and Fenn, R.: Models for the Aerosols of the Lower Atmosphere and the Effects of Humidity Variations on their Optical Properties, Environ. Res., 94, 1979.

Shi, W. and Wang, M.: Detection of turbid waters and absorbing aerosols for the MODIS ocean color data processing, Remote Sensing of Environment, 110, 149-161, https://doi.org/10.1016/j.rse.2007.02.013, 2007.

Stramski, D., Joshi, I., and Reynolds, R. A.: Ocean color algorithms to estimate the concentration of particulate organic carbon in surface waters of the global ocean in support of a long-term data record from multiple satellite missions, Remote Sensing of Environment, 269, 112776, https://doi.org/10.1016/j.rse.2021.112776, 2022.

Stramski, D., Reynolds, R. A., Kahru, M., and Mitchell, B. G.: Estimation of Particulate Organic Carbon in the Ocean from Satellite Remote Sensing, Science, 285, 239-242, doi:10.1126/science.285.5425.239, 1999.

Todd, R. E. and Ren, A. S.: Warming and lateral shift of the Gulf Stream from in situ observations since 2001, Nature Climate Change, 13, 1348-1352, 10.1038/s41558-023-01835-w, 2023.

Tong, Y., Feng, L., Zhao, D., Xu, W., and Zheng, C.: Remote sensing of chlorophyll-a concentrations in coastal oceans of the Greater Bay Area in China: Algorithm development and long-term changes, International Journal of Applied Earth Observation and Geoinformation, 112, 102922, https://doi.org/10.1016/j.jag.2022.102922, 2022.

Twedt, K., Xiong, X., Geng, X., Wilson, T., and Mu, Q.: Impact of satellite orbit drift on MODIS Earth scene observations used in calibration of the reflective solar bands, SPIE Optical Engineering + Applications, SPIE2023.

Wang, M. and Jiang, L.: Atmospheric Correction Using the Information From the Short Blue Band, IEEE Transactions on Geoscience and Remote Sensing, 56, 6224-6237, 10.1109/TGRS.2018.2833839, 2018.

Wang, M. and Shi, W.: Cloud Masking for Ocean Color Data Processing in the Coastal Regions, IEEE Transactions on Geoscience and Remote Sensing, 44, 3196-3105, 10.1109/TGRS.2006.876293, 2006.

Wang, M., Son, S., and Shi, W.: Evaluation of MODIS SWIR and NIR-SWIR atmospheric correction algorithms using SeaBASS data, Remote Sensing of Environment, 113, 635-644, 10.1016/j.rse.2008.11.005, 2009.

Wang, S., Li, X., Sun, D., He, X., Zhang, H., Zhao, W., and He, Y.: Satellite estimation of suspended particle types using a backscattering efficiency-based model in the marginal seas, Opt. Express, 31, 890-906, 10.1364/OE.476192, 2023.

Wang, Y., Wang, J., Levy, R. C., Xu, X., and Reid, J. S.: MODIS Retrieval of Aerosol Optical Depth over Turbid Coastal Water, Remote Sensing, 9, 595, 2017.

Wei, J., Wang, M., Jiang, L., Yu, X., Mikelsons, K., and Shen, F.: Global Estimation of Suspended Particulate Matter From Satellite Ocean Color Imagery, Journal of Geophysical Research: Oceans, 126, e2021JC017303, https://doi.org/10.1029/2021JC017303, 2021.

Werdell, P. J., Franz, B. A., and Bailey, S. W.: Evaluation of shortwave infrared atmospheric correction for ocean color remote sensing of Chesapeake Bay, Remote Sensing of Environment, 114, 2238-2247, https://doi.org/10.1016/j.rse.2010.04.027, 2010.

Werdell, P. J., Bailey, S., Fargion, G., Pietras, C., Knobelspiesse, K., Feldman, G., and McClain, C.: Unique data repository facilitates ocean color satellite validation, Eos, Transactions American Geophysical Union, 84, 377-387, https://doi.org/10.1029/2003EO380001, 2003.

https://doi.org/10.5194/essd-2025-438
Preprint. Discussion started: 13 August 2025

Werdell, P. J., Franz, B. A., Bailey, S. W., Feldman, G. C., Boss, E., Brando, V. E., Dowell, M., Hirata, T., Lavender, S. J., Lee, Z., Loisel, H., Maritorena, S., Mélin, F., Moore, T. S., Smyth, T. J., Antoine, D., Devred, E., d'Andon, O. H. F., and Mangin, A.: Generalized ocean color inversion model for retrieving marine inherent optical properties, Appl. Opt., 52, 2019-2037, 10.1364/AO.52.002019, 2013.

Xu, Y., Zhou, S., Hu, L., Wang, Y., and Xiao, W.: Different controls on sedimentary organic carbon in the Bohai Sea: River mouth relocation, turbidity and eutrophication, Journal of Marine Systems, 180, 1-8, https://doi.org/10.1016/j.jmarsys.2017.12.004, 2018.

Ye, H., Li, J., Li, T., Shen, Q., Zhu, J., Wang, X., Zhang, F., Zhang, J., and Zhang, B.: Spectral Classification of the Yellow Sea and Implications for Coastal Ocean Color Remote Sensing, Remote Sensing, 8, 321, 2016.

Yu, S., Bai, Y., He, X., Gong, F., and Li, T.: A new merged dataset of global ocean chlorophyll-a concentration for better trend detection, Frontiers in Marine Science, Volume 10 - 2023, 10.3389/fmars.2023.1051619, 2023.

Zhang, M., Ma, R., Li, J., Zhang, B., and Duan, H.: A Validation Study of an Improved SWIR Iterative Atmospheric Correction Algorithm for MODIS-Aqua Measurements in Lake Taihu, China, IEEE Transactions on Geoscience and Remote Sensing, 52, 4686-4695, 10.1109/TGRS.2013.2283523, 2014.

Zhao, D., Feng, L., and He, X.: Global Gridded Aerosol Models Established for Atmospheric Correction Over Inland and Nearshore Coastal Waters, Journal of Geophysical Research: Atmospheres, 128, e2023JD038815, https://doi.org/10.1029/2023JD038815, 2023.

Zhao, G., Jiang, W., Wang, T., Chen, S., and Bian, C.: Decadal Variation and Regulation Mechanisms of the Suspended Sediment Concentration in the Bohai Sea, China, Journal of Geophysical Research: Oceans, 127, e2021JC017699, https://doi.org/10.1029/2021JC017699, 2022.

Zhao, S., Wu, Y., Lv, J., Zhao, D., Zheng, Y., and Feng, L.: High-Quality Remote Sensing Reflectance Products over China and US Coast (MODIS, 2003-2022) [dataset], https://doi.org/10.5281/zenodo.16413443, 2025.

Zhou, Y., Levy, R. C., Remer, L. A., Mattoo, S., and Espinosa, W. R.: Dust Aerosol Retrieval Over the Oceans With the MODIS/VIIRS Dark Target Algorithm: 2. Nonspherical Dust Model, Earth and Space Science, 7, e2020EA001222, https://doi.org/10.1029/2020EA001222, 2020.